The IVIM signal in the healthy cerebral gray matter: a play of spherical and non-spherical components

Finkenstaedt, Tim ; Klarhoefer, Markus ; Eberhardt, Christian ; Becker, Anton S ; Andreisek, Gustav ; Boss, Andreas ; Rossi, Cristina

Abstract: The intra-voxel incoherent motion (IVIM) model assumes that blood flowing in isotropically distributed capillary segments induces a phase dispersion of the MR signal, which increases the signal attenuation in diffusion-weighted images. However, in most tissue types the capillary network has an anisotropic micro-architecture. In this study, we investigated the possibility to indirectly infer the anisotropy of the capillary network in the healthy cerebral gray matter by evaluating the dependence of the IVIM signal from the direction of the diffusion-encoding. Perfusion-related indices and self-diffusion were modelled as symmetric rank 2 tensors. The geometry of the tensors was quantified pixel-wise by decomposing the tensor in sphere-like, plane-like, and line-like components. Additionally, trace and fractional anisotropy of the tensors were computed. While the self-diffusion tensor is dominated by a spherical geometry with a residual contribution of the non-spherical components, both, fraction of perfusion and pseudo-diffusion, present a substantial (in the order of 30%) contribution of planar and linear components to the tensor metrics. This study shows that the IVIM perfusion estimates in the cerebral gray matter present a detectable deviation from the spherical model. These non-spherical components may reflect the direction-dependent morphology of the microcirculation. Therefore, the tensor generalization of the IVIM model may provide a tool for the non-invasive monitoring of cerebral capillary micro-architecture during development, aging or in pathologies.

DOI: https://doi.org/10.1016/j.neuroimage.2017.03.004

NeuroImage 152 (2017) 340–347

Contents lists available at ScienceDirect

NeuroImage

journal homepage: www.elsevier.com/locate/neuroimage

The IVIM signal in the healthy cerebral gray matter: A play of spherical and non-spherical components

Tim Finkenstaedt[a], Markus Klarhoefer[b], Christian Eberhardt[a], Anton S. Becker[a], Gustav Andreisek[a], Andreas Boss[a], Cristina Rossi[a,*]

[a] Institute of Diagnostic and Interventional Radiology, University Hospital Zurich, University of Zurich, Switzerland
[b] Siemens Healthcare AG, Zurich, Switzerland

ARTICLE INFO

Keywords:
IVIM
Tensor
Anisotropy
Gray matter

ABSTRACT

The intra-voxel incoherent motion (IVIM) model assumes that blood flowing in isotropically distributed capillary segments induces a phase dispersion of the MR signal, which increases the signal attenuation in diffusion-weighted images. However, in most tissue types the capillary network has an anisotropic micro-architecture. In this study, we investigated the possibility to indirectly infer the anisotropy of the capillary network in the healthy cerebral gray matter by evaluating the dependence of the IVIM signal from the direction of the diffusion-encoding.

Perfusion-related indices and self-diffusion were modelled as symmetric rank 2 tensors. The geometry of the tensors was quantified pixel-wise by decomposing the tensor in sphere-like, plane-like, and line-like components. Additionally, trace and fractional anisotropy of the tensors were computed.

While the self-diffusion tensor is dominated by a spherical geometry with a residual contribution of the non-spherical components, both, fraction of perfusion and pseudo-diffusion, present a substantial (in the order of 30%) contribution of planar and linear components to the tensor metrics.

This study shows that the IVIM perfusion estimates in the cerebral gray matter present a detectable deviation from the spherical model. These non-spherical components may reflect the direction-dependent morphology of the microcirculation. Therefore, the tensor generalization of the IVIM model may provide a tool for the non-invasive monitoring of cerebral capillary micro-architecture during development, aging or in pathologies.

Introduction

The Intra-voxel Incoherent Motion (IVIM) model (Le Bihan et al., 1988, 1986) ascribes the signal attenuation in diffusion-weighted images to two main components: a slow component, due to the water self-diffusion, i.e. due to the transport of water molecules within tissue water as a result of random molecular movements; and a fast component, due to the flow of water molecules in segments of the capillary network.

Generally, a random orientation of the capillary segments is assumed resulting in an isotropic contribution of the perfusion effects on the signal attenuation (Le Bihan et al., 1986; Le Bihan and Turner, 1992). To disentangle perfusion and diffusion effects, a high signal-to-noise ratio is required, and technical challenges such as artifacts from other bulk flow phenomena have to be overcome; a comprehensive review is provided by Iima (Iima and Le Bihan, 2016). The assumption of random orientation of capillaries is crucial for the interpretation of the IVIM signal attenuation in terms of perfusion estimates, as blood flow in randomly oriented linear capillary segments results in intra-voxel distribution of phase dispersions, and, in turn, in increased signal attenuation of the diffusion-weighted images (Le Bihan and Turner, 1992). However, this assumption does not account for the anisotropy of the microcirculation in most tissue types. A dependence of the IVIM parameters on the diffusion encoding direction could be demonstrated in the renal medulla suggesting that both, blood flow and tissue microarchitecture, contribute to the anisotropy of diffusion measurements in the kidneys (Hilbert et al., 2016; Notohamiprodjo et al., 2015). Models accounting for a partial orientation of the microcirculation have been proposed for the characterization of the signal pattern of diffusion-weighted images on skeletal muscles (Karampinos et al., 2010) and on the myocardium (Abdullah et al., 2015). A non-isotropic perfusion contribution to the diffusion-weighted signal would be in accordance with the morphometry of the microcirculation of the gray matter, which presents an orientation of the capillary network nearly

* Corresponding author.
E-mail address: cristina.rossi@usz.ch (C. Rossi).

http://dx.doi.org/10.1016/j.neuroimage.2017.03.004
Received 2 January 2017; Accepted 2 March 2017
Available online 03 March 2017

perpendicular to the surface of the sulci (Jones, 1970; Lauwers et al., 2008). The indirect assessment of the morphology of the microcirculation by IVIM could potentially provide a non-invasive tool for monitoring tissue microvascular growth and degeneration. Moreover, a direction-dependent influence of the perfusion on the signal may affect the quantification of the diffusion anisotropy in the tissue using conventional diffusion techniques.

The aim of this study was to investigate the full orientation dependence of the diffusion data in the human cerebral gray matter using a tensor formalism to all IVIM parameters.

Materials and methods

Subjects

Nine healthy volunteers (34 ± 12 years old, range: 22–64 years, 3 women, 6 men) were included in this prospective study. The study was approved by the local ethics committee. All participants gave written informed consent to the MR examinations and to the scientific evaluation of the data sets.

MRI

The MR data were acquired using a 3 T whole-body scanner (MAGNETOM Skyra, Siemens Healthcare, Erlangen, Germany). The MR signal was received using a 64-channel head coil, while the built-in body transmit coil was used for spin excitation.

A 3D T1-weighted MPRAGE sequence (TR=7 ms, TE=2.32 ms, flip angle=8°, TI=900 ms, parallel imaging using GRAPPA, acceleration factor 2) was acquired for anatomical orientation.

Diffusion-weighted images were acquired using a fat-saturated Echo Planar Imaging (EPI) sequence with twice refocused diffusion preparation (TR=4100 ms; TE=90 ms; echo spacing=0.68 ms; bandwidth in EPI readout direction=1685 Hz/px, GRAPPA acceleration factor=2; partial Fourier=7/8; voxel size=2×2×2 mm^3; number of slices=24; b-values: 0, 5, 10, 20, 35, 55, 80, 110, 150, 200, 300, 500, 750, 1000, 1300, 0, 110, 150, 200, 300, 500, 750, 1000 0, 0 s/mm^2, 20 diffusion-encoding directions). Acquisition time for the diffusion-weighted images was about 30 min.

Post-processing and computation of parametrical maps

Before computation of the parametric maps, diffusion-weighted volumes were realigned to the first b0-volume (Fig. 1) using the "diffusion" toolbox of SPM 12 (Statistical Parametrical Mapping 12, Wellcome Trust Centre for Neuroimaging, London, UK). For each diffusion-encoding direction and for each b-value higher than 110 s/mm^2, the diffusion-weighted images were acquired twice. For each diffusion-encoding direction, corresponding image volumes acquired with b-values higher than 110 s/mm^2 were averaged, after motion correction, to improve the signal-to-noise ratio (SNR) of the diffusion-weighted images (Fig. 1). DW-images were filtered with a 2D Gaussian smoothing operator (FWHM=4.7 mm) to reduce the effect of noise (Fig. 1).

Three-dimensional anatomical images were segmented into gray matter using the automated segmentation tool of SPM12 and then co-registered to the first b0-volume (Fig. 2).

The IVIM tensor model

The IVIM model describes the MR signal attenuation for increasing strength of the diffusion weighting in dependence of diffusion and perfusion-related parameters according to the following equation (Eq. (1)):

$$\frac{S_b}{S_0} = fe^{-b\bullet D^*} + (1-f)e^{-b\bullet D}. \quad (1)$$

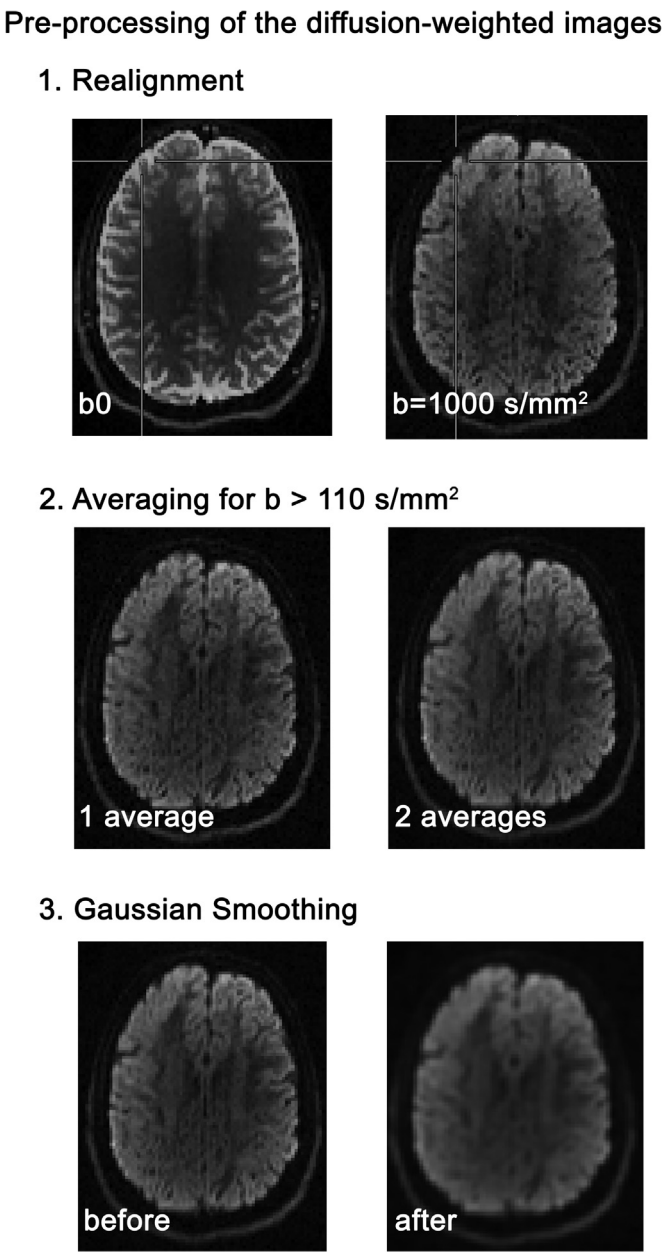

Fig. 1. Pre-processing steps of the diffusion-weighted images acquired for one representative volunteer (male, 31 years old). As a first, diffusion-weighted images were realigned to first b0 volume. Images acquired with b-values higher than 110 s/mm^2 were acquired twice and correspondingly averaged. Finally, Gaussian smoothing was performed to mitigate the effect of random noise.

In Eq. (1), S_b and S_O represent the signal intensity for a given b-value and for a b-value of 0 s/mm^2, respectively. The fraction of perfusion f (dimensionless index ranging between 0 and 1) indicates the relative amount of capillary water in the voxel. The pseudo-diffusion D^* (in units of mm^2/s) is a perfusion related component of the signal attenuation, which mimics the diffusion process. It depends on the mean length of the capillary segments and on the mean blood speed. The parameter D (in units of mm^2/s) is the self-diffusion coefficient of water in the tissue.

Tensor approaches have been proposed in other studies to model the direction-dependent attenuation of the IVIM signal (Abdullah et al., 2015; Karampinos et al., 2010; Notohamiprodjo et al., 2015). In this study all IVIM parameters were formalized as symmetric rank 2 tensors (Eberhardt, 2016; Hilbert et al., 2016).

The signal attenuation of Eq. (1) was generalized as:

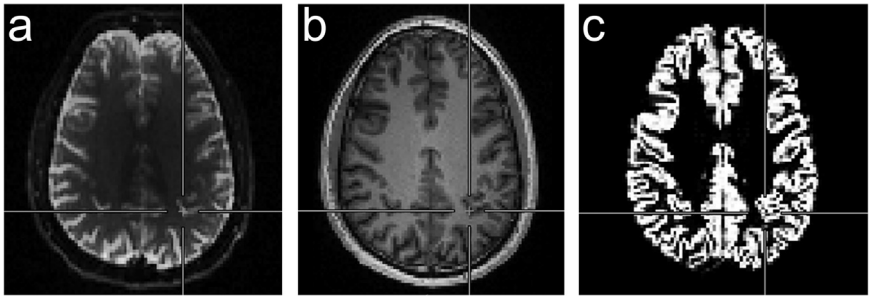

Fig. 2. Representative example of the co-registration of the T1-weighted anatomical volume (b) into the b0-volume (a). For this volunteer (male, 31 years old) the co-registered probability tissue map of gray matter (c) is reported as well. Cross lines are shown to help comparison between images.

$$\frac{S_b}{S_0} = (1 - \vec{g}^T \boldsymbol{f} \vec{g}) e^{-b\vec{g}^T \boldsymbol{D} \vec{g}} + \vec{g}^T \boldsymbol{f} \vec{g}\, e^{-b\vec{g}^T \boldsymbol{D^*} \vec{g}} \quad (2)$$

where $\vec{g}$ is the normalized diffusion-encoding gradient vector, b is the scalar nominal b-value, and $\boldsymbol{f}$, $\boldsymbol{D}$, and $\boldsymbol{D^*}$ are rank 2 tensors representing the fraction of perfusion, the self-diffusion, and the pseudo-diffusion, respectively.

The assumed anisotropy of the IVIM indexes implies that the result of the single measurement does not fully characterize the physical property within the sample but it represents the projection of the tensor along the direction of observation (Kingsley, 2006).

Signal processing over the motion-corrected DW-images was performed as following:

1) For each diffusion-encoding direction, the projections of the IVIM tensors were estimated from Eq. (2) using a step-wise approach (Patel et al., 2010)
   a) The diffusion coefficient, D, and the intercept of the high b-value fit to the b=0 s/mm^2, S_{int}, were estimated by linear fitting of the logarithm of the signal, S_b, for b-values higher than 200 s/mm^2 to the function: $\ln(S_b)=\ln(S_{int})-b \bullet D$;
   b) The fraction of perfusion, f, was approximated as: $f = \frac{S_0 - S_{int}}{S_0}$;
   c) The pseudo-diffusion coefficient, D^*, was subsequently estimated by bi-exponential fitting of the signal to Eq. (2) while keeping D and f constant as calculated in a) and b).
2) For each tensor, the 20 measured projections, **M** (vector of size 20×1), were related to the tensor elements, **E** (vector of size 6×1) via the **B**-matrix (matrix of size 20×6) (Basser et al., 1994), which depended on the diffusion-encoding scheme, as **M**=**B**x**E**, with "x" indicating the matrix product. Tensors elements were computed pixel-wise as $\mathbf{E}=\mathbf{B}^{-1}\mathrm{x}\mathbf{M}$, with $\mathbf{B}^{-1}=(\mathbf{B}^T\mathbf{B})^{-1}\mathbf{B}^T$. The derived tensors were then diagonalized.
3) For each tensor, the eigenvalues (λ_{max}, λ_{med}, λ_{min}) and the trace ($<\lambda>=(\lambda_{max}+\lambda_{med}+\lambda_{min})/3$) were computed. Westin anisotropy measures (Westin et al., 2002) ($c_S=\lambda_{min}/\lambda_{max}$, $c_P=(\lambda_{med}-\lambda_{min})/\lambda_{max}$, $c_L=(\lambda_{max}-\lambda_{med})/\lambda_{max}$), and fractional anisotropy (Basser, 1995) ($FA = \sqrt{\frac{3}{2}} \frac{\sqrt{(\lambda_{max}-\langle\lambda\rangle)^2+(\lambda_{med}-\langle\lambda\rangle)^2+(\lambda_{min}-\langle\lambda\rangle)^2}}{\sqrt{\lambda_{max}^2+\lambda_{med}^2+\lambda_{min}^2}}$) were computed for quantification of the geometrical properties of the derived tensors.

In the point 1, just the signal from b-values higher than 10 s/mm^2 was considered for the estimation of the perfusion indexes in order to minimize the contributions from gradients responsible for spatial encoding to the diffusion weighting.

A "difference method" (Price et al., 1990) based on the processing of two repeated acquisitions of the b0-volume was used for the estimation of the SNR of the diffusion-weighted dataset. For one representative subject, the SNR in the whole segmented gray matter was calculated as $SNR = \sqrt{2} \bullet m_{sum}/s_{diff}$, where m_{sum} is the mean value of the signal in the sum image and s_{diff} is the standard deviation (computed over the same ROI) of the signal in the difference image.

For each subject, mean values of the Westin measures, of the FA, and of the trace were computed, for each tensor, over the segmented gray matter. To reduce potential contamination of the cerebrospinal fluid (CSF), a mask of the gray matter was computed by setting to zero pixels of the segmented volume, which presented a probability of less than 90% for belonging to the gray matter tissue.

Westin measures of the three tensors were compared for statistical differences using a one sample t-test ($p < 0.05$). Tensor calculations were performed using in house custom software written in Matlab (MATLAB Release 2013b, The MathWorks, Inc., Natick, Massachusetts, United States). For each IVIM tensor, ellipsoid visualization was generated using the plotDTI function of Barmpoutis (Barmpoutis et al., 2007).

For each subject the mean angle between the directions of the main eigenvectors of the tensors were computed over the segmented gray matter. The relative angle, δ, between two main eigenvector directions ($\boldsymbol{\varepsilon}$ and $\boldsymbol{\eta}$) was computed as $\delta=\cos^{-1}(\boldsymbol{\varepsilon}\cdot\boldsymbol{\eta})$.

The direction-dependence of the IVIM signal was qualitatively estimated in one representative volunteer. Signal intensities were measured over one voxel of the segmented gray matter as a function of the b-values along two (orthogonal) directions, which were selected parallel and perpendicular to the main eigenvector of the fraction of perfusion tensor (Fig. 3).

For the same volunteer and for each tensor of the model, projections of the tensor along the diffusion-encoding directions were plotted as a function of the polar angle $\theta=\arccos(\boldsymbol{g}\bullet\boldsymbol{v})$ between the diffusion-encoding direction $\boldsymbol{g}$ and the direction $\boldsymbol{v}$ of the main eigenvector of the tensor (Fig. 4). The plots were generated as reported by (Notohamiprodjo et al., 2015). First, for each voxel of the whole segmented gray matter the **D**, **D***, and **f** projections were sorted as a function of the corresponding values of the polar angle. Second, the mean and the standard deviation (within angular bins of 5 degrees) were calculated. The standard error was computed as (standard deviation/number of points)$^{0.5}$ (Notohamiprodjo et al., 2015).

Error estimates

The degree to which image noise may affect tensor-derived quantities in the framework proposed in this study was estimated on a set of synthetic data.

One dataset representing a volume of 3×3 pixels was generated. The simulated volume contained three regions, which differed in the geometrical properties of the perfusion-related tensors (Fig. 5). In the first region, a spherical geometry of the perfusion-related tensors was assumed. The trace of the tensor was set to 0.12 for the fraction of perfusion and to $8{\cdot}10^{-3}$ mm^2/s for the pseudo-diffusion (Stieb et al., 2016). In the second region, a line-like metric was simulated, while in the third region a planar geometry was assumed for both perfusion indexes. The trace of each of the three tensors was kept equal in all three regions. In the whole volume, isotropic self-diffusion was assumed (Trace=$0.7{\cdot}10^{-3}$ mm^2/s). In the simulation, each tensor was perfectly aligned with the gradient reference frame.

Image noise was modeled assuming a Gaussian distribution with

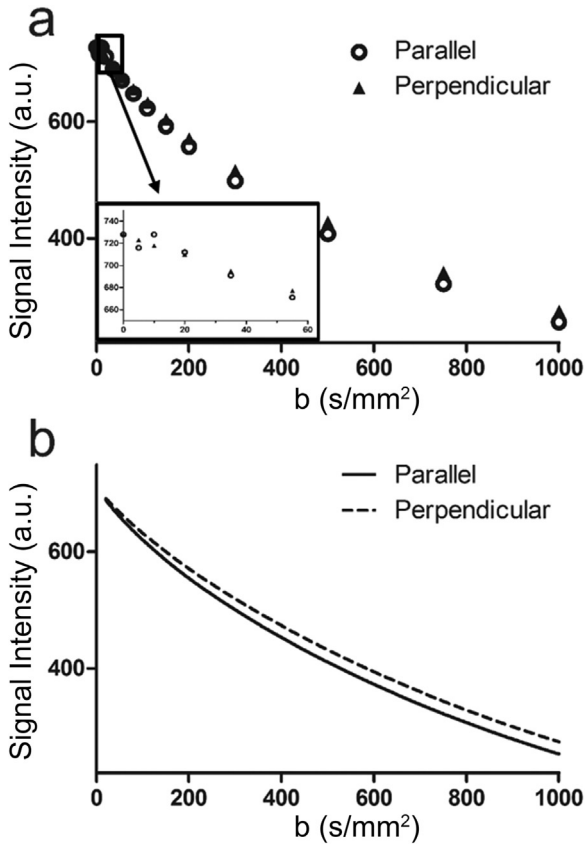

Fig. 3. Signal intensity vs. b-value strength for two diffusion-encoding directions parallel and perpendicular to the main eigenvector of the fraction of perfusion tensor in one representative voxel of the gray matter (a). In the zoomed portion of graph (a) (black rectangle) a deviation from the expected bi-exponential path for b-values lower than 10 s/mm^2, probably due to the coupling between the imaging and the diffusion-encoding gradients, is shown. Graph (b) shows the bi-exponential curves fitted through the measured points for b-values higher than 10 s/mm^2 (perpendicular direction: f=0.09, D*=9·10^{-3} mm^2/s, D=0.9·10^{-3} mm^2/s; parallel direction: f=0.11, D*=8·10^{-3} mm^2/s, D=0.9·10^{-3} mm^2/s).

variance σ^2 to the original signal S_O (Anderson, 2001; Taylor and Biswal, 2011). The noisy MR signal was approximated as (Gudbjartsson and Patz, 1995):

$$S_b^{Noise} = \sqrt{S_b^2 + \sigma^2}. \quad (3)$$

Tensor metrics were computed for the expected geometry, for noiseless signal (Eq. 2) and for the noisy signal (Eq. 3) for noise standard deviation, σ, equal to 0.2. The standard deviation was set to this value in order to simulate image noise in order of that measured over the dataset on healthy volunteers, according to the equation SNR=A/σ (Gudbjartsson and Patz, 1995), where A is the image pixel intensity in the absence of noise. Indexes of tensor metric computed over the synthetic data in the three cases (expected, noiseless, and noisy) were statistically compared using a two-tailed paired t-test ($p < 0.05$). The deviation of the estimated value (V) from the synthetic one was computed as $\Delta = (V_{Expected} - V_{Noisy/Noiseless})$.

Results

In all nine subjects, adequate image quality allowed the computation of the parameter maps in the segmented gray matter (Fig. 6).

Mean trace values for each of the computed tensors, as well as mean values of the Westin measures and of the fractional anisotropy (FA) are reported in Table 1. For the self-diffusion tensor, a mean trace of (0.91 ± 0.09) 10^{-3} mm^2/s was computed over the segmented gray matter. The mean trace of the pseudo-diffusion tensor measured (6.22 ± 0.48)

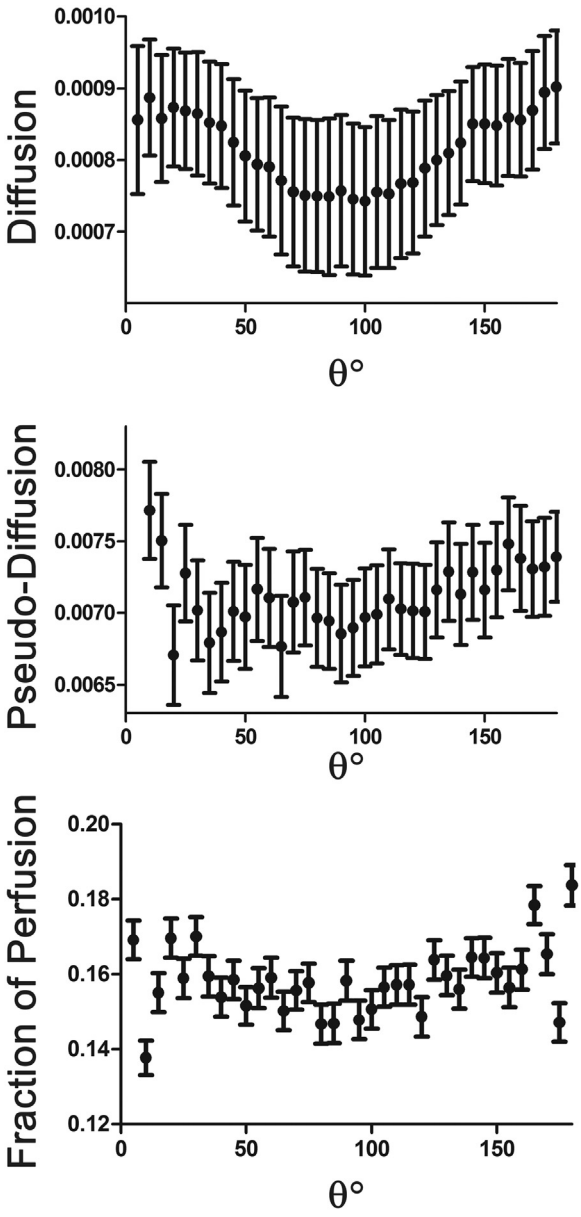

Fig. 4. For one representative volunteer and for each tensor, projections of the tensor along the diffusion-encoding directions were plotted as a function of the polar angle $\vartheta = \cos^{-1}(\boldsymbol{g} \bullet \boldsymbol{v})$ between the diffusion-encoding direction $\boldsymbol{g}$ and the direction $\boldsymbol{v}$ of the main eigenvector of the tensor. Each of the three IVIM indexes shows a dependence from the direction of diffusion-encoding. The characteristic pattern of the projections indicates a dominant anisotropy along the direction of the main eigenvector for each of the tensors.

10^{-3} mm^2/s, while a mean fraction of perfusion of (0.10 ± 0.03) was found in the cohort of subjects.

Westin measures showed a dominant spherical geometry of the diffusion tensor with a mean c_s of 0.77 ± 0.02. A weaker contribution of the planar (0.09 ± 0.01) and of the linear (0.14 ± 0.01) geometry was found (Table 1, Fig. 7). Also for the pseudo-diffusion and for the fraction of perfusion, the geometries of the tensors were dominated by the spherical component (pseudo-diffusion: c_S=0.56 ± 0.06; fraction of perfusion: c_S=0.52 ± 0.07). However, for the perfusion estimates, the contributions of the planar and of the linear components to the geometry of the tensors were significantly higher than in the case of the self-diffusion tensor ($p < 0.05$). The pseudo-diffusion tensor presented a mean planar component of 0.23 ± 0.07 and a mean linear component of 0.35 ± 0.06. A similar trend was found for the fraction of perfusion (c_P=0.29 ± 0.05; c_L=0.34 ± 0.06). Overall, the non-spherical components of the tensors measured 29 ± 9% for the pseudo-diffusion

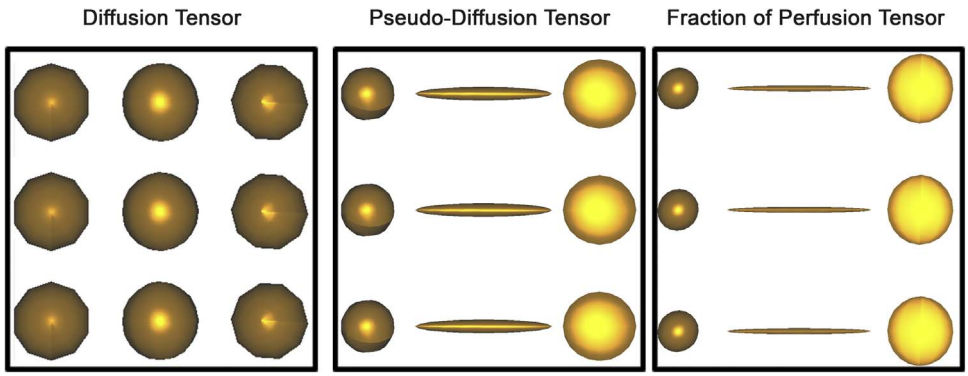

Fig. 5. Ellipsoid representation of the three tensors for the synthetic dataset used for the error estimation. Without the effect of noise, isotropic self-diffusion was expected within the whole volume, while the geometry of the perfusion-related tensors was assumed to change in the volume. Columns of the diagrams of the perfusion-related tensors correspond to three simulated phases (i.e. isotropic, axial, and planar). For each tensor, the size of the ellipsoid has been adjusted for visualization.

tensor, 31 ± 6% for the perfusion fraction tensor, and just 12 ± 3% for the diffusion tensor.

Relatively high eccentricity of the tensor was found for the fraction of perfusion (FA=0.38 ± 0.07) and for the pseudo-diffusion tensor (0.36 ± 0.07) (Table 1). The diffusion tensor presented fairly spherical geometry, as confirmed from a mean FA of 0.14 ± 0.02 (Table 1).

The ellipsoid visualization of the tensors' geometry reflected the anisotropy predicted by the Westins measurements and by the FA. Cigar-shaped ellipsoids were computed mostly in the gyri of the cortical gray matter for both the fraction of perfusion and the pseudo diffusion (Fig. 8). In most anatomical locations, the main axis of the pseudo-diffusion ellipsoid showed a nearly perpendicular orientation to the direction of the sulci (Fig. 8). For the same anatomical location, the main ellipsoid axis of the pseudo-diffusion tensor exhibited a nearly specular orientation as compared to the main axis of the fraction of perfusion tensor (Fig. 8), while the diffusion ellipsoid presented an almost spherical geometry. A mean relative angle of 71 ± 13 degrees was measured over the segmented gray matter between the main eigenvector of the fraction of perfusion tensor and the main eigenvector of the pseudo-diffusion tensor. The angles between the main eigenvectors measured 82 ± 4 degrees for the fraction of perfusion and the diffusion tensors, and 71 ± 12 degrees for the pseudo-diffusion and the diffusion tensors.

Error estimates

Simulations showed that both, the selected algorithm for computation of the IVIM parameters (Eq. (2)) and image noise, marginally contributed to the quantification of the metrics of the tensors (Table 2). Image noise resulted in a mean deviation of −0.02 ± 0.12 for the FA, while for the Westins measurements mean deviations ranged between −0.04 ± 0.14 and 0.03 ± 0.13. For each tensor, deviations from the expected values depended on the simulated geometry. Maximum deviations of the indexes from the expected values in the order of 10–13% were observed if a planar geometry was assumed. Milder deviations (mean deviations: 1–2%) were found otherwise. The estimation of the properties of the pseudo-diffusion tensor resulted to be more sensitive to the effect of noise in the case of planar geometry. In this case an overestimation of the planar component of the D* up to 34% was observed. Similar deviation patterns were observed when comparing the noiseless signal with the signal corrupted by Gaussian noise. However, no significant differences between the computed values (with and without the presence of noise) and the expected values were found (minimum p=0.19).

Discussion

In this study, we analyzed the orientation dependence of the IVIM signal in the cerebral gray matter and report normal values for healthy volunteers. For the perfusion-related IVIM parameters, a considerable deviation of the tensor geometry from the spherical model was measured. A main orientation of the perfusion-related tensors was observed nearly perpendicular to the sulci. This result is in accordance to *ex vivo* confocal laser microscopy measurements, which reported an angle of circa 80° between the main orientation of the gray matter capillary network and the surface of the sulcus (Lauwers et al., 2008). The tensor generalization of the IVIM model may reflect the anisotropy of the microcirculation.

Hilbert et al. (2016) recently suggested that the IVIM-tensor imaging of the kidneys potentially provides information on *architec-*

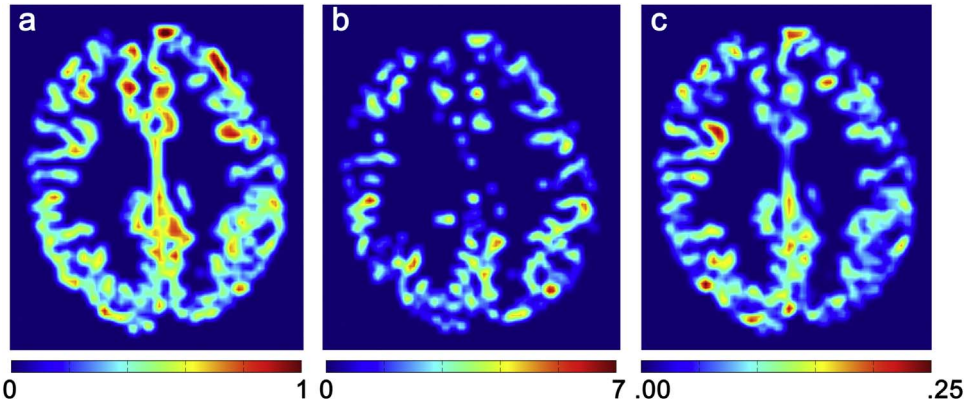

Fig. 6. Trace maps of the diffusion tensor (a), the pseudo-diffusion tensor (b) and the fraction of perfusion tensor (c) computed for one of the healthy volunteers (female, 22 years old) are reported for the segmented gray matter. The trace of the diffusion tensor (a) and of the pseudo-diffusion tensor (b) are reported in units of 10^{-3} mm^2/s. Fraction of perfusion (c) is a dimensionless index ranging between 0 and 1.

Table 1
Mean values (± standard deviation, SD) of the parametrical indexes computed for each of the three tensors over the segmented gray matter. The trace values for the diffusion and the pseudo-diffusion tensors are reported in units of 10^{-3} mm^2/s.
FA=Fractional anisotropy.

		Diffusion					Pseudo-Diffusion				Fraction of perfusion				
Vol	**Age**	**Spherical**	**Planar**	**Linear**	**Trace**	**FA**	**Spherical**	**Planar**	**Linear**	**Trace**	**FA**	**Spherical**	**Planar**	**Linear**	**Trace**	**FA**
1	22	0.79 ± 0.08	0.08 ± 0.05	0.12 ± 0.07	0.76 ± 0.09	0.12 ± 0.06	0.64 ± 0.17	0.16 ± 0.10	0.23 ± 0.18	5.21 ± 1.72	0.25 ± 0.15	0.64 ± 0.20	0.19 ± 0.16	0.22 ± 0.21	0.11 ± 0.07	0.25 ± 0.19
2	39	0.75 ± 0.14	0.11 ± 0.07	0.15 ± 0.11	0.89 ± 0.20	0.16 ± 0.11	0.46 ± 0.24	0.25 ± 0.18	0.38 ± 0.27	6.42 ± 1.35	0.45 ± 0.25	0.40 ± 0.22	0.36 ± 0.22	0.37 ± 0.24	0.07 ± 0.05	0.50 ± 0.24
3	37	0.77 ± 0.14	0.09 ± 0.07	0.13 ± 0.11	1.01 ± 0.27	0.14 ± 0.11	0.57 ± 0.44	0.41 ± 0.35	0.43 ± 0.36	6.46 ± 1.81	0.44 ± 0.33	0.49 ± 0.26	0.34 ± 0.26	0.36 ± 0.30	0.06 ± 0.06	0.42 ± 0.27
4	31	0.74 ± 0.15	0.11 ± 0.08	0.15 ± 0.11	0.90 ± 0.29	0.16 ± 0.11	0.59 ± 0.25	0.22 ± 0.20	0.35 ± 0.32	6.14 ± 1.82	0.35 ± 0.27	0.53 ± 0.24	0.29 ± 0.24	0.36 ± 0.29	0.12 ± 0.10	0.38 ± 0.25
5	64	0.79 ± 0.11	0.08 ± 0.06	0.13 ± 0.08	1.01 ± 0.30	0.12 ± 0.08	0.51 ± 0.24	0.21 ± 0.16	0.38 ± 0.30	6.58 ± 1.39	0.39 ± 0.25	0.51 ± 0.21	0.27 ± 0.19	0.29 ± 0.21	0.09 ± 0.05	0.37 ± 0.22
6	30	0.79 ± 0.12	0.08 ± 0.05	0.13 ± 0.10	0.92 ± 0.19	0.13 ± 0.09	0.61 ± 0.22	0.18 ± 0.16	0.29 ± 0.26	6.86 ± 0.98	0.30 ± 0.23	0.51 ± 0.19	0.27 ± 0.18	0.30 ± 0.22	0.09 ± 0.06	0.37 ± 0.20
7	34	0.74 ± 0.16	0.11 ± 0.09	0.15 ± 0.13	0.81 ± 0.20	0.16 ± 0.13	0.52 ± 0.25	0.24 ± 0.20	0.36 ± 0.28	6.28 ± 1.59	0.40 ± 0.27	0.46 ± 0.21	0.32 ± 0.19	0.37 ± 0.30	0.09 ± 0.07	0.43 ± 0.23
8	28	0.78 ± 0.15	0.09 ± 0.07	0.13 ± 0.12	0.94 ± 0.31	0.14 ± 0.11	0.62 ± 0.25	0.21 ± 0.20	0.34 ± 0.32	5.86 ± 1.85	0.33 ± 0.28	0.59 ± 0.25	0.25 ± 0.23	0.36 ± 0.34	0.11 ± 0.10	0.35 ± 0.27
9	25	0.74 ± 0.10	0.10 ± 0.06	0.13 ± 0.12	0.94 ± 0.31	0.14 ± 0.11	0.56 ± 0.25	0.20 ± 0.18	0.36 ± 0.31	6.20 ± 1.70	0.38 ± 0.27	0.51 ± 0.23	0.28 ± 0.22	0.42 ± 0.36	0.15 ± 0.14	0.39 ± 0.26
Mean	**±SD**	**34 ± 12**	**0.77 ± 0.02**	**0.09 ± 0.01**	**0.14 ± 0.01**	**0.91 ± 0.09**	**0.14 ± 0.02**	**0.56 ± 0.06**	**0.23 ± 0.07**	**0.35 ± 0.06**	**6.22 ± 0.48**	**0.36 ± 0.07**	**0.52 ± 0.07**	**0.29 ± 0.05**	**0.34 ± 0.06**	**0.10 ± 0.03**	**0.38 ± 0.07**

Fig. 7. For each tensor, parametrical measures of anisotropy are depicted for one of the volunteers (female, 30 years old). For each of the tensors, the gray matter presented a dominant sphere-like geometry. However, for the perfusion-related tensors plane-like and line-like geometries were detected.

Fig. 8. For each tensor, ellipsoidal representations are depicted for a rectangular region-of-interest (red rectangle over the axial T1-weighted anatomical reference image). While the self-diffusion tensor mostly shows a spherical geometry of the tensor, both, the pseudo-diffusion and the fraction of perfusion, are characterized by cigar-shaped ellipsoids. The direction of the main axes of the ellipsoids is nearly perpendicular to the sulci. A specular symmetry between the main axes of the pseudo-diffusion and of the perfusion fraction tensors was found in several anatomical areas. For each tensor the size of the ellipsoid has been adjusted for visualization.

tural anisotropy (via the $\boldsymbol{f}$ tensor) and on *functional* anisotropy (via the $\boldsymbol{D}^*$ tensor). In our study, quantitative measurements of the geometry of the tensor showed a similar pattern for the pseudo-diffusion and the perfusion fraction, which suggests reasonable correlation between the geometric orientation of the microvessels and the net blood flow of the

Table 2
Expected values of the anisotropy indexes for a synthetic dataset and corresponding values computed with the Eq. (2) in the case of noiseless data and in the presence of image noise. FA=Fractional anisotropy.

		FA			Spherical			Linear			Planar		
		Exp.	Noiseless	Noisy	Exp.	Noiseless	Noisy	Exp.	Noiseless	Noisy	Exp.	Noiseless	Noisy
Geometry 1	D isotropic	0.00	0.00	0.00	1	1.00	1.00	0	0.00	0.00	0	0.00	0.00
	D* isotropic	0.00	0.00	0.00	1	1.00	1.00	0	0.00	0.00	0	0.00	0.00
	f isotropic	0.00	0.00	0.00	1	1.00	1.00	0	0.00	0.00	0	0.00	0.00
Geometry 2	D isotropic	0.00	0.01	0.08	1	0.98	0.86	0	0.00	0.01	0	0.02	0.13
	D* axial symmetry	1.00	0.87	0.79	0	0.10	0.18	1	0.87	0.81	0	0.03	0.01
	f axial symmetry	1.00	0.96	1.00	0	0.04	0.00	1	0.96	1.00	0	0.00	0.00
Geometry 3	D isotropic	0.00	0.01	0.00	1	0.99	0.94	0	0.01	0.06	0	0.00	0.00
	D* planar symmetry	0.41	0.52	0.45	0	0.25	0.34	0	0.01	0.00	1	0.74	0.66
	f planar symmetry	0.41	0.60	0.67	0	0.15	0.06	0	0.00	0.00	1	0.85	0.94

microcirculation. However, a mostly specular symmetry of the main tensor eigenvector was found when comparing $\boldsymbol{D}^*$ and $\boldsymbol{f}$ in the same anatomical location (Fig. 8). A mean angle of 71 ± 13 degrees was measured over the gray matter between the main eigenvector directions of the two tensors $\boldsymbol{D}^*$ and $\boldsymbol{f}$. This result may reflect the coupling between the geometry of the capillary network along a certain diffusion-encoding direction and the signal attenuation. The study of Hilbert et al. (2016) dealing with the anisotropic IVIM signal of the kidneys proposes four different scenarios for the interpretation of the biophysical meaning of the anisotropic flow (I: mean speed of flowing spins is equal along all directions and number of vessels is equal along all directions, D* and f are both isotropic; II: mean speed is higher in one direction, while the number of vessels is the same along all directions, D* is anisotropic while f is isotropic; III: more vessels are aligned to one direction, while mean speeds are equal along all directions, so f is anisotropic while D* is isotropic; IV: all vessels are aligned towards a preferred main direction, so both D* and f are anisotropic). In our study, and in other studies (Eberhardt et al., 2016; Wurnig et al., 2015), we observed that large D* values often correspond to low f values. In our study, although both indexes result in an anisotropic behavior, the geometry of the tensors is not the same (as it would be in the case of the scenario IV). Our results suggest a fifth possible scenario that is not contemplated in the work of Hilbert et al., i.e. the case of high velocity components along few capillary segments.

The analysis of the trace of the three tensors is in agreement with the values reported in the literature for the gray matter using a segmented algorithm (Stieb et al., 2016; Wu et al., 2015). In our study a low fractional anisotropy of the diffusion tensor was measured over the gray matter as compared to the values reported in the literature (Lawrenz et al., 2016). Generally, the estimation of the diffusion properties in the tissue using Diffusion Tensor Imaging (DTI) relies on the computation of an apparent diffusion tensor, which contains the contribution of further sources of intra-voxel dephasing than the pure self-diffusion of the water molecules. Hilbert et al. (2016) recently proved that the fractional anisotropy of the diffusion in kidneys is overestimated if the perfusion contribution on the signal attenuation is discarded. Moreover, a b-value dependence of the FA estimates using DTI was reported in mice (Hui et al., 2010), which again suggests the critical role of perfusion in the estimation of the diffusion properties. These results may explain the discrepancy we found between our values and the ones previously reported in the literature.

Validity of the model

In this study we proposed a generalization of the IVIM model (Le Bihan et al., 1986). The original IVIM model attributes the signal attenuation at low b-values to one main vascular pool and to self-diffusion. However, in principle a distribution of pseudo-diffusion values should be expected depending on the morphometry of the capillaries and on the blood velocity in the capillary segments. In other organs, as for example the liver, not only the capillary blood flow but also other sources of intra-voxel incoherent motion (e.g. water diffusion in the gallbladder) probably contribute to the attenuation of the DW-signal for low b-values (Pazahr et al., 2014). This shows that the original IVIM model surely relays on a simplification. Measurements performed at ultra-high field strength showed that for short echo-times a second vascular pool is detectable in the brain (Fournet et al., 2016). In the clinical setting of this study, the echo time was set to the minimum value possible for the bipolar diffusion preparation. A further reduction of the echo time could be possible using a monopolar spin echo preparation. However, in this case potential artifacts due to incompletely canceled eddy currents could occur (Alexander et al., 1997).

In our study, we propose a rank-2 tensor model for each of the IVIM indexes. Similarly to the case of the apparent diffusion tensor of rank 2, this model indirectly assumes that one main orientation affects the MR signal attenuation within the voxel (orientational homogeneity). Several studies performed in the past showed that in the case of an expected orientational heterogeneity (e.g. in the case of white matter fibers crossing within the voxel) higher rank tensor models better describe the diffusion-weighted signal pattern (Ozarslan and Mareci, 2003). Although our model seems to improve the original formulation of the IVIM signal in the gray matter (which relied on a rank-0 tensor model), discarding higher rank tensor contribution may have led to residual bias in the signal characterization.

Study limitations

Although cerebral gray matter segmentation was performed to reduce the contamination of the Cerebral Spinal Fluid (CSF), the slightly higher trace of the diffusion tensor measured in this study over the segmented gray matter compared to other studies suggests a potential overestimation of the diffusivity due to partial volume effects near the cortical surface (Zacharopoulos and Narayana, 1998). Scalar values of the IVIM parameters reported elsewhere computed by suppressing the CSF signal are slightly lower than the trace values reported in this study (Federau et al., 2014). The extend of the CSF contribution on the reported anisotropy measurements could be assessed by testing the TE dependence of the IVIM parameters computed over the gray matter (Bisdas and Klose, 2015). Alternatively, CSF contamination may be reduced by incorporating a fluid attenuation inversion recovery (FLAIR) preparation into the diffusion-weighted sequence (Zacharopoulos and Narayana, 1998). Recently, a T2-prepared inversion recovery acquisition was proposed to reduce CSF contamination, which was demonstrated to provide a higher recovery of arterial and venous blood magnetization compared

to standard inversion recovery techniques (Federau and O'Brien, 2015). A further limitation is related to the estimation of the fraction of perfusion. To account for the effect of the imaging gradients over the effective diffusion-encoding, tensor computations were performed by using the b-matrix provided by the vendor. For b-values lower than 5 s/mm^2, a deviation of the signal from the biexponential pattern was observed. To avoid detrimental effects on the estimation of the perfusion indices, the S_0 signal at the step 1b of the computation was approximated with the signal measured at b=10 s/mm^2. Therefore, a slight underestimation of the perfusion fraction may have occurred. The third limitation concerns the algorithm used for computation of the projections of the three tensors along the single diffusion-encoding directions. In this study, a segmented least square approach was applied. The segmented approach was selected as a robust alternative to the conventional biexponential least-squares fit. The segmented algorithm assumes that for b-values higher than a certain threshold diffusion dominates the signal of the DW-images. However, a main limitation of this strategy is that a single b-value threshold is used for the whole-tissue computation without accounting for potential differences in tissue perfusion due to anatomy of function (Wurnig et al., 2015). A further point concerns the computation of the mean angle between the two main eigenvectors of the perfusion-related tensors. In this study, for each volunteer, the mean angle was computed over all voxels of the segmented gray matter. Therefore, the mean value reported in the manuscript includes the contribution of well-perfused voxel and of less perfused ones. Moreover, although image quality was good and images were acquired above the lateral ventricles to avoid susceptibility artifacts close to the nose cavity or skull base, we cannot exclude a residual detrimental effect due to overfitting or local signal voids. Fig. 4 shows that image noise residually affects the estimation of perfusion anisotropy in vivo. The diagram computed over one representative volunteer presents large jumps between neighboring bins around 0° and 180° for both the perfusion-related tensors. Moreover, a slight deviation from the expected half-peanut results in a certain asymmetry of the curves around the 90°.

In conclusion, we could prove that the IVIM signal in the cerebral gray matter is direction-dependent. The anisotropy of the perfusion-related parameters may reflect the net microarchitecture of the human cerebral gray matter microvasculature as well as the inherent flow characteristics of its microcirculation. Thus, IVIM tensor imaging may serve as a new tool for the assessment of cerebral microvascular growth and degeneration.

Acknowledgement

The authors are grateful to Prof. Uwe Klose and to Dr. Ana-Maria Oros-Peusquens for suggestions and discussions. Preliminary results of this study were presented at the ESMRMB 2016.

References

Abdullah, O.M., Gomez, A.D., Merchant, S., Heidinger, M., Poelzing, S., Hsu, E.W., 2015. Orientation dependence of microcirculation-induced diffusion signal in anisotropic tissues. Magn. Reson. Med..

Alexander, A.L., Tsuruda, J.S., Parker, D.L., 1997. Elimination of eddy current artifacts in diffusion-weighted echo-planar images: the use of bipolar gradients. Magn. Reson. Med. 38, 1016–1021.

Anderson, A.W., 2001. Theoretical analysis of the effects of noise on diffusion tensor imaging. Magn. Reson. Med. 46, 1174–1188.

Barmpoutis, A., Vemuri, B.C., Shepherd, T.M., Forder, J.R., 2007. Tensor splines for interpolation and approximation of DT-MRI with applications to segmentation of isolated rat hippocampi. IEEE Trans. Med. Imaging 26, 1537–1546.

Basser, P.J., 1995. Inferring microstructural features and the physiological state of tissues from diffusion-weighted images. NMR Biomed. 8, 333–344.

Basser, P.J., Mattiello, J., LeBihan, D., 1994. Estimation of the effective self-diffusion tensor from the NMR spin echo. J. Magn. Reson. B 103, 247–254.

Bisdas, S., Klose, U., 2015. IVIM analysis of brain tumors: an investigation of the relaxation effects of CSF, blood, and tumor tissue on the estimated perfusion fraction. MAGMA 28, 377–383.

Eberhardt, C., Finkenstaedt, K.M., Andreisek, T., Boss, G., Rossi C, A., 2016. Orientation dependence of the IVIM signal in the healthy cerebral gray matter. Magn. Reson. Mater. Phys. Biol. Med., 29.

Federau, C., O'Brien, K., 2015. Increased brain perfusion contrast with T(2)-prepared intravoxel incoherent motion (T2prep IVIM) MRI. NMR Biomed. 28, 9–16.

Federau, C., O'Brien, K., Meuli, R., Hagmann, P., Maeder, P., 2014. Measuring brain perfusion with intravoxel incoherent motion (IVIM): initial clinical experience. J. Magn. Reson Imaging 39, 624–632.

Fournet, G., Li, J.R., Cerjanic, A.M., Sutton, B.P., Ciobanu, L., Le Bihan, D., 2016. A two-pool model to describe the IVIM cerebral perfusion. J. Cereb. Blood Flow Metab..

Gudbjartsson, H., Patz, S., 1995. The Rician distribution of noisy MRI data. Magn. Reson. Med. 34, 910–914.

Hilbert, F., Bock, M., Neubauer, H., Veldhoen, S., Wech, T., Bley, T.A., Kostler, H., 2016. An intravoxel oriented flow model for diffusion-weighted imaging of the kidney. NMR Biomed. 29, 1403–1413.

Hui, E.S., Cheung, M.M., Chan, K.C., Wu, E.X., 2010. B-value dependence of DTI quantitation and sensitivity in detecting neural tissue changes. Neuroimage 49, 2366–2374.

Iima, M., Le Bihan, D., 2016. Clinical intravoxel incoherent motion and diffusion MR imaging: past. Present Future Radiol. 278, 13–32.

Jones, E.G., 1970. On the mode of entry of blood vessels into the cerebral cortex. J. Anat. 106, 507–520.

Karampinos, D.C., King, K.F., Sutton, B.P., Georgiadis, J.G., 2010. Intravoxel partially coherent motion technique: characterization of the anisotropy of skeletal muscle microvasculature. J. Magn. Reson Imaging 31, 942–953.

Kingsley, P.B., 2006. Introduction to diffusion tensor imaging mathematics: Part I. Tensors, rotations, and eigenvectors. Concepts Magn. Reson. Part A 28A, 101–122.

Lauwers, F., Cassot, F., Lauwers-Cances, V., Puwanarajah, P., Duvernoy, H., 2008. Morphometry of the human cerebral cortex microcirculation: general characteristics and space-related profiles. Neuroimage 39, 936–948.

Lawrenz, M., Brassen, S., Finsterbusch, J., 2016. Microscopic diffusion anisotropy in the human brain: age-related changes. Neuroimage 141, 313–325.

Le Bihan, D., Breton, E., Lallemand, D., Aubin, M.L., Vignaud, J., Laval-Jeantet, M., 1988. Separation of diffusion and perfusion in intravoxel incoherent motion MR imaging. Radiology 168, 497–505.

Le Bihan, D., Breton, E., Lallemand, D., Grenier, P., Cabanis, E., Laval-Jeantet, M., 1986. MR imaging of intravoxel incoherent motions: application to diffusion and perfusion in neurologic disorders. Radiology 161, 401–407.

Le Bihan, D., Turner, R., 1992. The capillary network: a link between IVIM and classical perfusion. Magn. Reson. Med. 27, 171–178.

Notohamiprodjo, M., Chandarana, H., Mikheev, A., Rusinek, H., Grinstead, J., Feiweier, T., Raya, J.G., Lee, V.S., Sigmund, E.E., 2015. Combined intravoxel incoherent motion and diffusion tensor imaging of renal diffusion and flow anisotropy. Magn. Reson. Med. 73, 1526–1532.

Ozarslan, E., Mareci, T.H., 2003. Generalized diffusion tensor imaging and analytical relationships between diffusion tensor imaging and high angular resolution diffusion imaging. Magn. Reson. Med. 50, 955–965.

Patel, J., Sigmund, E.E., Rusinek, H., Oei, M., Babb, J.S., Taouli, B., 2010. Diagnosis of cirrhosis with intravoxel incoherent motion diffusion MRI and dynamic contrast-enhanced MRI alone and in combination: preliminary experience. J. Magn. Reson. Imaging 31, 589–600.

Pazahr, S., Nanz, D., Rossi, C., Chuck, N., Stenger, I., Wurnig, M.C., Schick, F., Boss, A., 2014. Magnetic resonance imaging of the liver: apparent diffusion coefficients from multiexponential analysis of b values greater than 50 s/mm^2 do not respond to caloric intake despite increased portal-venous blood flow. Invest. Radiol. 49, 138–146.

Price, R.R., Axel, L., Morgan, T., Newman, R., Perman, W., Schneiders, N., Selikson, M., Wood, M., Thomas, S.R., 1990. Quality assurance methods and phantoms for magnetic resonance imaging: report of AAPM nuclear magnetic resonance Task Group No. 1. Med. Phys. 17, 287–295.

Stieb, S., Boss, A., Wurnig, M.C., Ozbay, P.S., Weiss, T., Guckenberger, M., Riesterer, O., Rossi, C., 2016. Non-parametric intravoxel incoherent motion analysis in patients with intracranial lesions: test-retest reliability and correlation with arterial spin labeling. Neuroimage Clin. 11, 780–788.

Taylor, P.A., Biswal, B., 2011. Geometric analysis of the b-dependent effects of Rician signal noise on diffusion tensor imaging estimates and determining an optimal b value. Magn. Reson. Imaging 29, 777–788.

Westin, C.F., Maier, S.E., Mamata, H., Nabavi, A., Jolesz, F.A., Kikinis, R., 2002. Processing and visualization for diffusion tensor MRI. Med. Image Anal. 6, 93–108.

Wu, W.-C., Chen, Y.-F., Tseng, H.-M., Yang, S.-C., My, P.-C., 2015. Caveat of measuring perfusion indexes using intravoxel incoherent motion magnetic resonance imaging in the human brain. Eur. Radiol. 25, 2485–2492.

Wurnig, M.C., Donati, O.F., Ulbrich, E., Filli, L., Kenkel, D., Thoeny, H.C., Boss, A., 2015. Systematic analysis of the intravoxel incoherent motion threshold separating perfusion and diffusion effects: proposal of a standardized algorithm. Magn. Reson. Med. 74, 1414–1422.

Zacharopoulos, N.G., Narayana, P.A., 1998. Selective measurement of white matter and gray matter diffusion trace values in normal human brain. Med. Phys. 25, 2237–2241.